Organic Electronics 26 (2015) 239–244

Contents lists available at ScienceDirect

Organic Electronics

journal homepage: www.elsevier.com/locate/orgel

Letter

High-resolution spatial control of the threshold voltage of organic transistors by microcontact printing of alkyl and fluoroalkylphosphonic acid self-assembled monolayers

Ikue Hirata [a,*], Ute Zschieschang [b], Tomoyuki Yokota [a], Kazunori Kuribara [c], Martin Kaltenbrunner [d], Hagen Klauk [b], Tsuyoshi Sekitani [e], Takao Someya [a]

[a] Department of Applied Physics, The University of Tokyo, Tokyo, Japan
[b] Max Planck Institute for Solid State Research, Stuttgart, Germany
[c] Advanced Industrial Science and Technology, Japan
[d] Johannes Kepler University Linz, Austria
[e] Osaka University, Japan

ARTICLE INFO

Article history:
Received 28 March 2015
Received in revised form 19 June 2015
Accepted 14 July 2015

ABSTRACT

A dense array of 500 organic TFTs with two different threshold voltages arranged in a checkerboard pattern has been fabricated. The threshold voltages were defined by preparing self-assembled monolayers (SAMs) of either an alkyl or a fluoroalkylphosphonic acid on the gate-oxide surface of each TFT, using a combination of microcontact printing from an elastomeric stamp and dipping into a solution. The threshold voltages are −1.01 ± 0.15 V for the TFTs with the fluoroalkyl SAM and −1.28 ± 0.23 V for the TFTs with the alkyl SAM. ToF-SIMS analysis shows that the two SAMs can be patterned with a pitch of 10 μm and without significant cross-contamination. Cross-sectional TEM and NEXAFS characterization of the SAMs indicate that the properties of the SAMs prepared by microcontact printing and dipping are essentially identical.

1. Introduction

Continuous improvements in the performance, reproducibility, and reliability of organic thin-film transistors (TFTs) have recently fueled the development of more complex applications for organic TFTs, such as flexible and stretchable active-matrix displays [1,2], microprocessors [3], radio-frequency identification (RFID) tags [4], and sensor arrays [5,6].

An important requirement for the realization of robust integrated circuits based on organic TFTs is the ability to control the electrical properties of the TFTs. For example, in static random access memory (SRAM), the ability to set the threshold voltage of each TFT of the memory cells individually can greatly enhance the static noise margin and can be helpful in suppressing inadvertent switching events.

The threshold voltage of organic TFTs can be controlled, for example, by adjusting the thickness of the gate dielectric [7], by introducing controlled channel doping [8], by implementing a floating-gate structure [9], or by functionalizing the surface of the gate oxide with an organic self-assembled monolayer (SAM) [10]. The use of SAMs appears particularly promising, because of the availability of a wide range of SAMs with different properties [11,12], the reproducibility and tunability of the process [13,14], and the excellent stability of the SAMs [15,16]. Depending on the chemical structure of the SAM and the specific interactions at the interface between the SAM and the organic semiconductor, the threshold voltage of the TFTs is affected by the dipole moment of the SAM and/or by the space-charge layer induced by the SAM, so that depending on the combination of SAM and organic semiconductor, a robust, permanent and well-defined shift of the threshold voltage can be obtained [17].

The most popular method for preparing SAMs is by dipping the substrate into a liquid solution of the self-assembling molecules, which leads to the chemisorption of the molecules on the surface of the substrate and the spontaneous formation of a well-ordered monolayer [10–18]. A fundamental limitation of the dipping method is that it usually covers the entire substrate with the same SAM, making it difficult to create a dense pattern of more than one type of SAM on the same substrate. However, for certain applications, such as complementary circuits based on p-channel and n-channel organic TFTs that benefit from different gate-oxide modifications for each type of TFT [19], it is beneficial to be able to pattern more than one type of SAM on the same substrate. This will require the spatially resolved formation of each SAM on the

* Corresponding author at: Center for Nano Science and Technology, Italian Institute of Technology, Milan, Italy.
E-mail address: hirata@ntech.t.u-tokyo.ac.jp (I. Hirata).

http://dx.doi.org/10.1016/j.orgel.2015.07.031
1566-1199/

substrate, which can be accomplished, for example, by microcontact printing [20–23], microwriting [24], lithography with ultraviolet radiation [25], or combinations thereof [26].

Controlling the threshold voltages of organic TFTs in a complex pattern for large-scale integrated circuits requires a precise and deterministic process that can be applied to individual transistors with micron-scale resolution over large areas. In a previous study we demonstrated the formation of two different SAMs (an alkyl and a fluoroalkylphosphonic acid SAM) on the same substrate by microcontact printing [27], but with limited resolution and without the ability to pattern the SAMs in an arbitrary geometry.

Here we report on the fabrication and characterization of a dense array of 500 organic TFTs using two different patterned SAMs, so that each TFT has one of two different threshold voltages, depending on the type of SAM prepared on the gate-oxide surface of that transistor. The first SAM was prepared by microcontact printing, and the second SAM was prepared by dipping. A lateral resolution of 5 μm was achieved, and no significant contamination of the SAMs was observed by time-of-flight secondary ion mass spectrometry (ToF-SIMS).

2. Experimental

Five different alkyl and fluoroalkylphosphonic acids with three different chain lengths were employed in this work: *n*-octylphosphonic acid (HC_8-PA), *n*-decylphosphonic acid (HC_{10}-PA), *n*-tetradecylphosphonic acid (HC_{14}-PA), 3,3,4,4,5,5,6,6,7,7,8,8,8-terdecylfluoro-*n*-octylphosphonic acid (FC_8-PA) and 3,3,4,4,5,5,6,6,7,7,8,8,9,9,10,10,10-heptadecylfluoro-*n*-decylphosphonic acid (FC_{10}-PA).

Microcontact printing was performed using a polydimethylsiloxane (PDMS) stamp with raised and recessed regions arranged in a checkerboard pattern with a pitch of either 10 μm (for the structural characterization of the SAMs) or 3–4 mm (for the TFT array). To fabricate the stamp, a layer of a positive photoresist (JSR-PFR 7790G-27cp) was spin-coated onto an oxidized silicon wafer (spin-coating conditions: 700 rpm for 1 s, followed by 2000 rpm for 30 s) and baked at a temperature of 110 °C for 90 s. This silicon wafer serves as the master for the fabrication of the PDMS stamp. The photoresist was exposed to a checkerboard pattern using an LED Maskless Lithography System (PMT Cooperation) at the scan speed of 0.6 mm/s. The resist pattern was developed in an aqueous solution of tetramethyl ammonium hydroxide (2.38% NMD) for 60 s. After rinsing with pure deionized water, the resist was baked at a temperature of 110 °C for 200 s and coated with a fluoropolymer to facilitate the later release of the PDMS mold. PDMS diluted with hexane was then poured onto the resist pattern, degassed, and vulcanized at room temperature. Finally, the PDMS stamp was peeled from the silicon master.

An array of 500 organic TFTs with a pitch identical to that of the PDMS stamp and covering an area of 4×4 cm^2 was fabricated on a 50 μm thick flexible polyimide substrate. The TFTs were fabricated in the bottom-gate, top-contact device structure. 40 nm thick aluminum gate electrodes were deposited by thermal evaporation in vacuum through a shadow mask. The surface of the aluminum gate electrodes was exposed to a oxygen plasma to form a 4 nm thick layer of aluminum oxide (AlO_x). The freshly grown AlO_x surface is characterized by a large density of hydroxyl groups, thus providing an excellent template for the formation of high-quality phosphonic acid SAMs [15,16,27]. FC_8-PA and HC_8-PA SAMs were chosen for the TFTs, because in a preliminary experiment, TFTs with these two SAMs had shown better electrical performance than TFTs with FC_{10}-PA and HC_{10}-PA SAMs (see Fig. S2 and Table S1).

The process to pattern the two SAMs on the same substrate by a combination of microcontact printing (for the first SAM) and dipping (for the second SAM) is illustrated in Fig. 1. To prepare the first SAM, the PDMS stamp was immersed into a 2-propanol solution of FC_8-PA (1 mM) for 5 min, then dried with nitrogen. The stamp was then aligned with respect to the array of gate electrodes on the polyimide substrate and brought into contact with the substrate for 10 min. This leads to the transfer and chemisorption of FC_8-PA molecules from the raised regions of the stamp onto the surface of the plasma-oxidized gate electrodes, thus covering the gate electrodes of half of the TFTs of the array with FC_8-PA molecules. After removing the PDMS stamp from the substrate, the substrate was immersed into a 2-propanol solution of HC_8-PA (1 mM) overnight. This leads to the self-assembly of an HC_8-PA monolayer on those plasma-oxidized gate electrodes that had not been previously covered with FC_8-PA molecules during the microcontact-printing step, thus producing a checkerboard pattern of TFTs with FC_8-PA and HC_8-PA SAMs. Finally, the substrate was rinsed with 2-propanol and annealed at a temperature of 100 °C for 10 min in order to stabilize the monolayers [28].

After the formation of the two SAMs, a 30 nm thick layer of the small-molecule organic semiconductor dinaphtho[2,3-b:2′,3′-f]thieno[3,2-b]thiophene (DNTT) [29,30] and 50 nm thick Au source and drain contacts were vacuum-deposited through shadow masks. The TFTs have a channel length of approximately 40 μm and a channel width of 1000 μm. All electrical measurements were performed in ambient air at room temperature.

3. Structural characterization of the SAMs

Cross-sectional transmission electron microscopy (TEM), time-of-flight secondary ion mass spectroscopy (ToF-SIMS) and near-edge X-ray absorption fine structure (NEXAFS) spectroscopy were performed to characterize the morphology, the molecular composition and the molecular orientation of the SAMs. For these experiments, the SAMs were prepared on silicon substrates covered with a 100 nm thick layer of thermally grown SiO_2, a 40 nm thick layer of aluminum, and a 4 nm thick layer of oxygen-plasma-grown AlO_x.

The cross-sectional TEM images were obtained using a Hitachi High-Tech H-9000UHR microscope at an acceleration voltage of 300 kV. Fig. 2a shows the cross section through a Si/SiO_2/Al/AlO_x/SAM stack with an HC_{14}-PA SAM prepared by microcontact printing, Fig. 2b shows the cross section through a Si/SiO_2/Al/AlO_x/ SAM stack with an HC_{14}-PA SAM prepared by dipping, and Fig. 2c shows the cross section through a Si/SiO_2/Al/AlO_x stack without SAM. Although the interface between the AlO_x layer and the SAM is difficult to discern, the images indicate that the total dielectric thickness is larger by about 1 nm in Fig. 2a and b than in Fig. 2c. The thickness of the HC_{14}-PA SAMs is expected to be about 1.7 nm [31], *i.e.*, 70% larger than the increase in thickness indicated by the TEM cross-sectional images, but this deviation may be due to the fact that the interfaces between the various layers are not perfectly smooth, that the density of the SAM is smaller than that of the layers below and above the SAM, and that the TEM image is the result of electron absorption along the entire thickness of the specimen. Both the SAM prepared by microcontact printing and the SAM prepared by dipping appear continuous and without apparent defects.

Fig. 3 shows ToF-SIMS images of a checkerboard pattern of an FC_{10}-PA SAM prepared by microcontact printing followed by the preparation of an HC_{10}-PA SAM by dipping. The checkerboard pattern has a pitch of 10 μm. Fig. 3a–c show the spatial distributions of the measured intensities of the $Al_3O_6H_2$ signal, the F signal and the CH signal on the substrate surface, respectively. In principle, there are two conceivable contamination paths: one is the unintended desorption of the first SAM from the AlO_x surface during the dipping process (during which the second SAM is formed), and the other is the unintended adsorption of molecules during the dipping process onto the first SAM (formed previously by

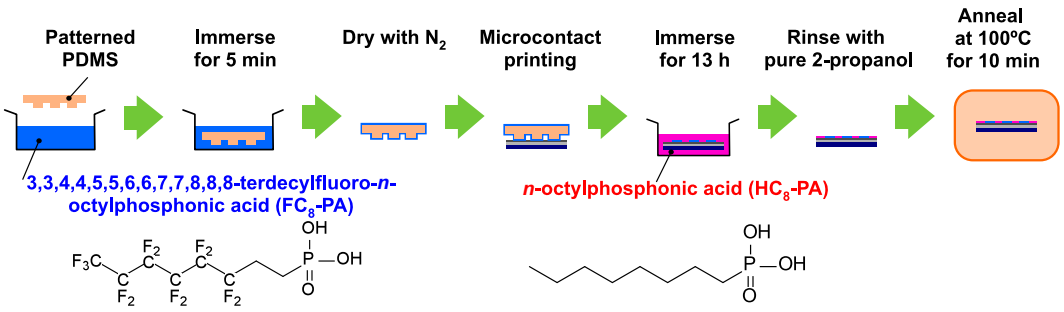

Fig. 1. Process flow for the preparation of a high-resolution checkerboard pattern of two different SAMs on the same substrate. First, a patterned PDMS stamp is immersed into a 2-propanol solution (1 mM) of the first molecule (FC_8-PA), so that the molecules are adsorbed on the stamp. The molecules are then transferred from the raised regions of the stamp to the substrate by microcontact printing, leading to the formation of a patterned FC_8-PA SAM on the substrate. The substrate is then immersed into a 2-propanol solution (1 mM) of the second molecule (HC_8-PA), resulting in the formation of an HC_8-PA SAM in those regions of the substrate not covered with an FC_8-PA SAM. Finally, the substrate is rinsed with pure 2-propanol and annealed at a temperature of 100 °C for 10 min.

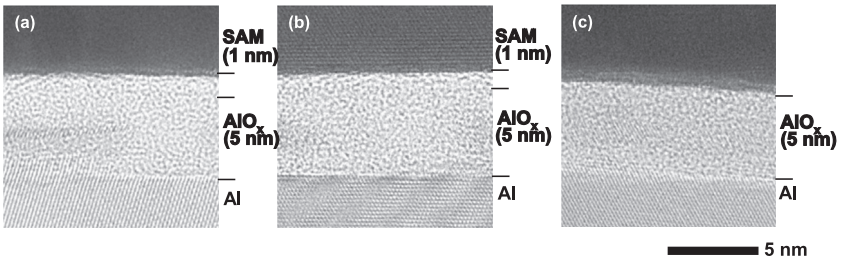

Fig. 2. Cross-sectional TEM images of the gate dielectric. (a) Cross section through a $Si/SiO_2/Al/AlO_x$/SAM stack with an HC_{14}-PA SAM prepared by microcontact printing. (b) Cross section through a $Si/SiO_2/Al/AlO_x$/SAM stack with an HC_{14}-PA SAM prepared by dipping. (c) Cross section through a $Si/SiO_2/Al/AlO_x$ stack without SAM.

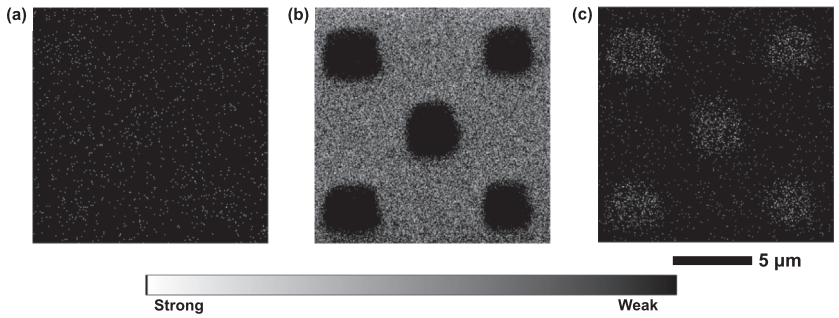

Fig. 3. ToF-SIMS images of a checkerboard pattern of an FC_{10}-PA SAM prepared by microcontact printing, followed by an HC_{10}-PA SAM prepared by dipping. The checkerboard pattern has a pitch of 10 µm. (a) Intensity distribution of the $Al_3O_6H_2$ signal. (b) Intensity distribution of the F signal. (c) Intensity distribution of the CH signal.

microcontact printing). However, in Fig. 3b and c, the intended checkerboard pattern produced by microcontact printing of the FC_{10}-PA SAM followed by the preparation of the HC_{10}-PA SAM by dipping is clearly recognized, and it can be seen that the areas with large intensities of the F and CH signals are complementary, without visible overlap or cross-contamination.

For comparison, ToF-SIMS images of a checkerboard pattern of an FC_{10}-PA SAM prepared by microcontact printing (not followed by the preparation of a second SAM) are shown in Fig. S1a–c. Comparing Figs. S1b and 3b, it can be seen that the intensity of the F signal in the microcontact-printed regions in Fig. S1b is stronger than the intensity of the F signal in the microcontact-printed regions in Fig. 3b; the reason is that in Fig. 3b, the substrate was rinsed with pure 2-propanol after the final process step, whereas rinsing was omitted in Fig. S1b. This illustrates the importance of performing a final rinsing step.

Furthermore, ToF-SIMS images of a checkerboard pattern of HC_{10}-PA and FC_{10}-PA SAMs prepared in the reverse order (*i.e.*, alkyl SAM prepared by microcontact printing in the first step, followed by preparing the fluoroalkyl SAM by dipping) are shown in Fig. S1d–f. Comparing Fig. S1e and Fig. 3b, it can be seen that the areas in which the HC_{10}-PA SAM was prepared by microcontact printing in Fig. S1e are slightly contaminated with fluorine, whereas the areas in which the HC_{10}-PA SAM was prepared by dipping in Fig. 3b are very clean. This suggests that some contamination occurred due to the unintended adsorption of FC_{10}-PA molecules onto the existing HC_{10}-PA SAM during dipping (Fig. S1e), whereas no contamination occurred when the FC_{10}-PA SAM was prepared first, followed by the preparation of the HC_{10}-PA SAM by dipping. Therefore, the latter sequence was chosen for the fabrication of the TFT array.

NEXAFS spectroscopy was performed to examine whether the orientation of the molecules within the SAM is affected by the method by which the SAMs are prepared. From NEXAFS measurements performed on SAMs based on *n*-octadecylphosphonic acid (HC_{18}–PA) prepared by dipping, Kuribara et al. previously

determined a dichroic ratio of 0.5–0.6, corresponding to a tilt angle of about 14–16° from the surface normal for the molecules in these SAMs [15].

Fig. 4a–c shows the NEXAFS partial electron yield spectra acquired for X-ray incident angles of 75°, 55°, and 35° on HC_{14}-PA SAMs prepared on $Si/SiO_2/Al/AlO_x$ substrates by three different protocols: Microcontact printing followed by rinsing with 2-propanol and annealing at a temperature of 100 °C (sample 1; Fig. 4a), microcontact printing without rinsing or annealing (sample 2; Fig. 4b), and dipping followed by rinsing and annealing (sample 3; Fig. 4c). The spectra are very similar to those reported by Kuribara et al. [15]. The signal peaks measured at an energy of 287.8 eV correspond to the C1s to σ^* transitions attributed to C–H bonds. From the integrated intensities of the σ^*_{C-H} resonance at 287.8 eV, virtually identical dichroic ratios of 0.39–0.40 were extracted from all spectra, indicating an approximately upright orientation of the HC_{14}-PA molecules regardless of the preparation method.

In Fig. 4d, the intensities of the spectra at post-edge 318 eV of the three different samples are compared. As can be seen, the intensities measured for sample 1 (microcontact printing followed by rinsing and annealing) and sample 3 (dipping followed by rinsing and annealing) are very similar, whereas the intensity measured for sample 2 (microcontact printing without rinsing or annealing) is notably larger, which indicates the presence of excess molecules not incorporated into the SAM on sample 2 and confirms the importance of rinsing and annealing after microcontact printing.

4. Transistor characteristics

An array of 500 organic TFTs was fabricated on flexible polyimide foil. Fig. 5a and b show photographs of one of the transistors and of the array. The electrical TFT characteristics were measured in ambient air at room temperature using a semiconductor parameter analyzer (Agilent B1500). Fig. 5c shows the distribution of the threshold voltage across the array of 500 TFTs. It can be clearly seen that the threshold voltage alternates between two distinct values along each row and each column of the array, confirming that the two SAMs (FC_8-PA and HC_8-PA) indeed form the intended checkerboard pattern. Fig. 5d shows representative transfer curves of a TFT with an FC_8-PA SAM (formed by microcontact printing) and of a TFT with an HC_8-PA SAM (formed by dipping). The threshold voltages and carrier mobilities extracted from the transfer curves are −1.10 V and 1.63 cm^2/Vs for the TFT with the FC_8-PA SAM and −1.29 V and 1.76 cm^2/Vs for the TFT with the HC_8-PA SAM. These carrier mobilities are very similar to those previously reported for DNTT TFTs fabricated on polyimide substrates [15,32], which indicates that the process for the patterning of the SAMs described here does not impair the carrier mobility of the TFTs.

The transfer curves of all 500 TFTs are shown in Fig. S3, and the histograms of the threshold voltages and the carrier mobilities extracted from all 500 TFTs are shown in Fig. 5e and f. 467 of the 500 TFTs (*i.e.*, 93%) were found to be functional. The average threshold voltage is −1.01 ± 0.15 V for the TFTs with the FC_8-PA SAM and −1.28 ± 0.23 V for the TFTs with the HC_8-PA SAM, and the average carrier mobility is 1.37 ± 0.38 cm^2/Vs for the TFTs with the FC_8-PA SAM and 1.76 ± 0.52 cm^2/Vs for the TFTs with the HC_8-PA SAM. The spatial distributions of the carrier mobility and on/off current ratio across the array are shown in Fig. S4a and b.

Figs. 5e and S4a indicate that the carrier mobility of the TFTs with the FC_8-PA SAM is smaller by about 20% than the mobility of the TFTs with the HC_8-PA SAM. The fact that the mobility of the TFTs with the fluoroalkyl SAM is somewhat smaller than the mobility of the TFTs with the alkyl SAM is consistent with similar observations reported in the literature for various organic semiconductors [11–14,19,27]. One explanation that has been put

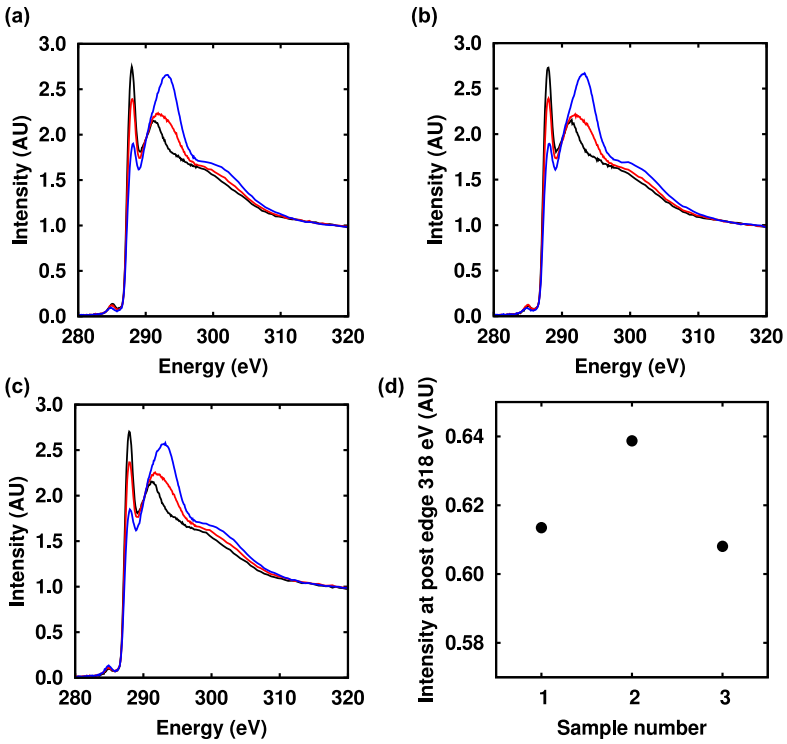

Fig. 4. NEXAFS characterization of the SAMs. (a) NEXAFS spectra of an HC_{14}-PA SAM prepared by microcontact printing, followed by rinsing with 2-propanol and annealing at 100 °C. The X-ray incident angle is 75° (black curve), 55° (red curve), and 35° (blue curve). (b) NEXAFS spectra of an HC_{14}-PA SAM prepared by microcontact printing without rinsing or annealing. (c) NEXAFS spectra of an HC_{14}-PA SAM prepared by dipping, followed by rinsing with 2-propanol and annealing at 100 °C. (d) Intensities of the NEXAFS spectra in the post-edge region (318 eV) of HC_{14}-PA SAMs prepared by microcontact printing with rinsing and annealing (sample 1), by microcontact printing without rinsing or annealing (sample 2), and by dipping with rinsing and annealing (sample 3). (For interpretation of the references to color in this figure legend, the reader is referred to the web version of this article.)

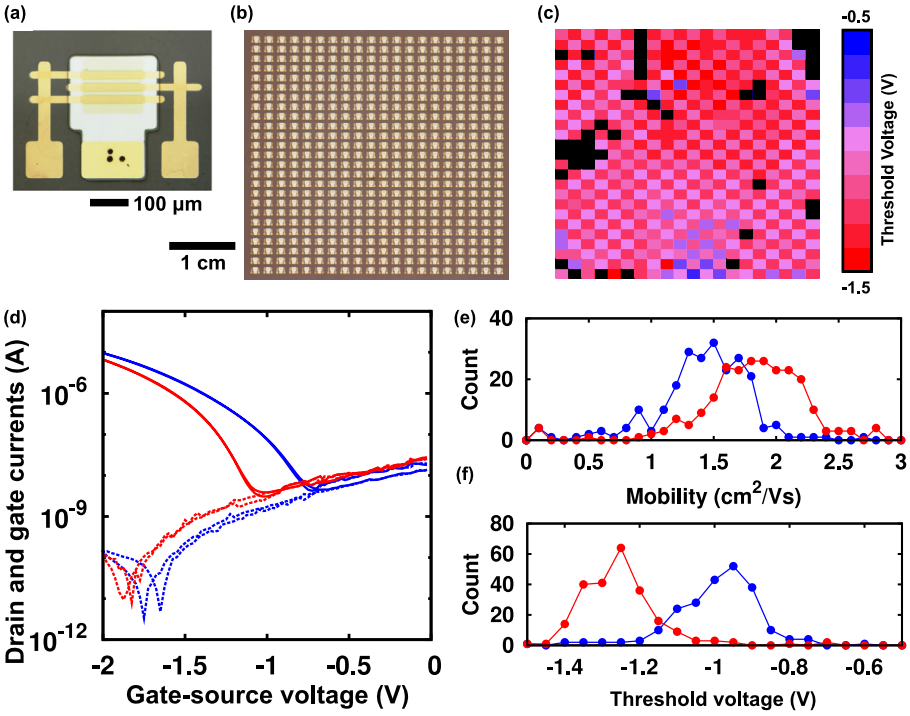

Fig. 5. Electrical characterization of the organic transistors. (a and b) Photographs of an individual TFT and of an array of 500 TFTs. (c) Distribution of the threshold voltage across the array of 500 TFTs. (d) Representative transfer curves of a TFT with an FC_8-PA SAM prepared by microcontact printing (blue curves) and of a TFT with an HC_8-PA SAM prepared by dipping (red curves). Solid lines indicate the drain currents, dotted lines the gate currents. (e and f) Histograms of the carrier mobilities and threshold voltages of 250 TFTs with an FC_8-PA SAM (blue data points) and 250 TFTs with an HC_8-PA SAM (red data points). (For interpretation of the references to color in this figure legend, the reader is referred to the web version of this article.)

forward by Mityashin et al. based on results from a multiscale modeling study is related to the observation that the energetic disorder in the organic semiconductor layer is notably larger when the semiconductor is deposited onto a fluoroalkyl SAM, as opposed to an alkyl SAM [33], and that this larger energetic disorder leads to a smaller carrier mobility [34].

5. Discussion

From the cross-sectional TEM and NEXAFS characterization of the SAMs, it is inferred that the structural properties of the SAMs are essentially identical, regardless of whether they were prepared by microcontact printing or by dipping. This confirms the chemisorption of the phosphonic acid molecules from the PDMS stamp onto the substrate surface and the formation of a self-assembled monolayer with an approximately upright orientation of the molecules.

Although the ToF-SIMS analysis indicates that there may be a small amount of contamination under certain conditions (*i.e.*, when a substrate covered with an alkylphosphonic acid SAM is dipped into a solution of a fluoroalkylphosphonic acid; see Fig. S1e), the analysis also shows that this contamination path can be avoided simply by first preparing the fluoroalkylphosphonic acid SAM and then the alkylphosphonic acid SAM (see Fig. 3). The ToF-SIMS results also indicate that there is no discernable contamination from the microcontact printing itself (see Figs. 3b and S1b). This is consistent with the very small surface-diffusion distance (100 nm) that has been reported for microcontact-printed alkanethiol SAMs [35], which is much smaller than the feature size of our TFTs (tens of microns). The same study [35] also showed that vapor-phase transport of the self-assembling molecules from the recessed regions of the stamp onto the substrate surface is negligible as well. The fact that the cross-contamination during the successive preparation of the SAMs is insignificant is reflected in the fact that we have been able to obtain a checkerboard pattern of two distinct, well-defined threshold voltages in an array of 500 TFTs (see Fig. 5c).

6. Conclusion

In conclusion, we have fabricated a dense array of 500 organic TFTs with spatially controlled threshold voltages defined using patterned alkyl and fluoroalkylphosphonic acid SAMs prepared by a combination of microcontact printing and dipping. The average threshold voltages are -1.01 ± 0.15 V for the TFTs with the fluoroalkyl SAM and -1.28 ± 0.23 V for the TFTs with the alkyl SAM. ToF-SIMS analysis shows that the SAMs can be patterned with a pitch of 10 µm and without significant cross-contamination. Cross-sectional TEM and NEXAFS characterization of the SAMs indicate that the properties of the SAMs prepared by microcontact printing and dipping are essentially identical.

Acknowledgments

This research was supported by the New Energy and Industrial Technology Development Organization (NEDO), the Project for Developing Innovation Systems of the Ministry of Education, Culture, Sports, Science and Technology (MEXT), and a Grant-in-Aid for Japan Society for the Promotion of Science (JSPS) Fellows Japan (Grant Number 251366). I.H. is grateful to the Research Fellowships for Young Scientists of JSPS.

Appendix A. Supplementary data

Supplementary data associated with this article can be found, in the online version, at http://dx.doi.org/10.1016/j.orgel.2015.07.031.

References

[1] T. Sekitani, Y. Noguchi, K. Hata, T. Fukushima, T. Aida, T. Someya, A rubberlike stretchable active matrix using elastic conductors, Science 321 (2008) 1468–1472, http://dx.doi.org/10.1126/science.1160309.

[2] S. Steudel, K. Myny, S. Schols, P. Vicca, S. Smout, A. Tripathi, et al., Design and realization of a flexible QQVGA AMOLED display with organic TFTs, Org. Electron. Phys. Mater. Appl. 13 (2012) 1729–1735, http://dx.doi.org/10.1016/j.orgel.2012.05.034.

[3] K. Myny, E. Van Veenendaal, G.H. Gelinck, J. Genoe, W. Dehaene, P. Heremans, et al., An 8-bit, 40-instructions-per-second organic microprocessor on plastic foil, IEEE J. Solid-State Circuits 47 (2012) 284–291, http://dx.doi.org/10.1109/JSSC.2011.2170635.

[4] K. Myny, S. Steudel, S. Smout, P. Vicca, F. Furthner, B. Van Der Putten, et al., Organic RFID transponder chip with data rate compatible with electronic product coding, Org. Electron. 11 (2010) 1176–1179, http://dx.doi.org/10.1016/j.orgel.2010.04.013.

[5] T. Someya, T. Sekitani, S. Iba, Y. Kato, H. Kawaguchi, T. Sakurai, A large-area, flexible pressure sensor matrix with organic field-effect transistors for artificial skin applications, Proc. Natl. Acad. Sci. U.S.A. 101 (2004) 9966–9970, http://dx.doi.org/10.1073/pnas.0401918101.

[6] T. Someya, Y. Kato, T. Sekitani, S. Iba, Y. Noguchi, Y. Murase, H. Kawaguchi, T. Sakurai, Conformable, flexible, large-area networks of pressure and thermal sensors with organic transistor active matrixes, Proc. Natl. Acad. Sci. U.S.A. 102 (2005) 12321–12325, http://dx.doi.org/10.1073/pnas.0502392102.

[7] H. Kawaguchi, M. Taniguchi, T. Kawai, Control of threshold voltage and hysteresis in organic field-effect transistors, Appl. Phys. Lett. 94 (2009) 093305/1–093305/3, http://dx.doi.org/10.1063/1.3095501.

[8] Y. Abe, T. Hasegawa, Y. Takahashi, T. Yamada, Y. Tokura, Control of threshold voltage in pentacene thin-film transistors using carrier doping at the charge-transfer interface with organic acceptors, Appl. Phys. Lett. 87 (2005) 153506/1–153506/3, http://dx.doi.org/10.1063/1.2099540.

[9] T. Yokota, T. Nakagawa, T. Sekitani, Y. Noguchi, K. Fukuda, U. Zschieschang, H. Klauk, K. Takeuchi, M. Takamiya, T. Sakurai, T. Someya, Control of threshold voltage in low-voltage organic complementary inverter circuits with floating gate structures, Appl. Phys. Lett. 9 (2011) 193302/1–193302/3, http://dx.doi.org/10.1063/1.3589967.

[10] S. Kobayashi, T. Nishikawa, T. Takenobu, S. Mori, T. Shimoda, T. Mitani, H. Shimotani, N. Yoshimoto, S. Ogawa, Y. Iwasa, Control of carrier density by self-assembled monolayers in organic field-effect transistors, Nat. Mater. 3 (2004) 317–322, http://dx.doi.org/10.1038/nmat1105.

[11] K.P. Pernstich, S. Haas, D. Oberhoff, C. Goldmann, D.J. Gundlach, B. Batlogg, A.N. Rashid, G. Schitter, Threshold voltage shift in organic field effect transistors by dipole monolayers on the gate insulator, J. Appl. Phys. 96 (2004) 6431–6438, http://dx.doi.org/10.1063/1.1810205.

[12] M. Salinas, C.M. Jäger, A.Y. Amin, P.O. Dral, T. Meyer-Friedrichsen, A. Hirsch, et al., The relationship between threshold voltage and dipolar character of self-assembled monolayers in organic thin-film transistors, J. Am. Chem. Soc. 134 (2012) 12648–12652, http://dx.doi.org/10.1021/ja303807u.

[13] U. Kraft, U. Zschieschang, F. Ante, D. Kälblein, C. Kamella, K. Amsharov, M. Jansen, K. Kern, E. Weber, H. Klauk, Fluoroalkylphosphonic acid self-assembled monolayer gate dielectrics for threshold-voltage control in low-voltage organic thin-film transistors, J. Mater. Chem. 20 (2010) 6416–6418, http://dx.doi.org/10.1039/c0jm01292k.

[14] U. Zschieschang, F. Ante, M. Schlörholz, M. Schmidt, K. Kern, H. Klauk, Mixed self-assembled monolayer gate dielectrics for continuous threshold voltage control in organic transistors and circuits, Adv. Mater. 22 (2010) 4489–4493, http://dx.doi.org/10.1002/adma.201001502.

[15] K. Kuribara, H. Wang, N. Uchiyama, K. Fukuda, T. Yokota, U. Zschieschang, C. Jaye, D. Fischer, H. Klauk, T. Yamamoto, K. Takimiya, M. Ikeda, H. Kuwabara, T. Sekitani, Y.L. Loo, T. Someya, Organic transistors with high thermal stability for medical applications, Nat. Commun. 3 (2012) 723, http://dx.doi.org/10.1038/ncomms1721.

[16] T. Yokota, K. Kuribara, T. Tokuhara, U. Zschieschang, H. Klauk, K. Takimiya, Y. Sadamitsu, M. Hamada, T. Sekitani, T. Someya, Flexible low-voltage organic transistors with high thermal stability at 250 °C, Adv. Mater. 25 (2013) 3639–3644, http://dx.doi.org/10.1002/adma.201300941.

[17] S.K. Possanner, K. Zojer, P. Pacher, E. Zojer, F. Schürrer, Threshold voltage shifts in organic thin-film transistors due to self-assembled monolayers at the dielectric surface, Adv. Funct. Mater. 19 (2009) 958–967, http://dx.doi.org/10.1002/adfm.200801466.

[18] A. Ulman, Formation and structure of self-assembled monolayers, Chem. Rev. 96 (1996) 1533–1554, http://dx.doi.org/10.1021/cr9502357.

[19] U. Kraft, M. Sejfic, M.J. Kang, K. Takimiya, T. Zaki, F. Letzkus, J.N. Burghartz, E. Weber, H. Klauk, Flexible low-voltage organic complementary circuits: finding the optimum combination of semiconductors and monolayer gate dielectrics, Adv. Mater. 27 (2015) 207–214, http://dx.doi.org/10.1002/adma.201403481.

[20] A. Kumar, H.A. Biebuyck, N.L. Abbott, G.M. Whitesides, The use of self-assembled monolayers and a selective etch to generate patterned gold features, J. Am. Chem. Soc. 114 (1992) 9188–9189, http://dx.doi.org/10.1021/ja00049a061.

[21] Y. Xia, M. Mrksich, E. Kim, G.M. Whitesides, Microcontact printing of octadecylsiloxane on the surface of silicon dioxide and its application in microfabrication, J. Am. Chem. Soc. 117 (1995) 9576–9577, http://dx.doi.org/10.1021/ja00142a031.

[22] N.L. Jeon, K. Finnie, K. Branshaw, R.G. Nuzzo, Structure and stability of patterned self-assembled films of octadecyltrichlorosilane formed by contact printing, Langmuir 13 (1997) 3382–3391, http://dx.doi.org/10.1021/la970166m.

[23] U. Zschieschang, M. Halik, H. Klauk, Microcontact-printed self-assembled monolayers as ultrathin gate dielectrics in organic thin-film transistors and complementary circuits, Langmuir 24 (2008) 1665–1669, http://dx.doi.org/10.1021/la703818d.

[24] A. Kumar, N.L. Abbott, H.A. Biebuyck, E. Kim, G.M. Whitesides, Patterned self-assembled monolayers and meso-scale phenomena, Acc. Chem. Res. 28 (1995) 219–226, http://dx.doi.org/10.1021/ar00053a003.

[25] H. Sugimura, K. Ushiyama, A. Hozumi, O. Takai, Micropatterning of alkyl- and fluoroalkylsilane self-assembled monolayers using vacuum ultraviolet light, Langmuir 16 (2000) 885–888, http://dx.doi.org/10.1021/jp034665+.

[26] A. Kumar, H.A. Biebuyck, G.M. Whitesides, Patterning self-assembled monolayers: applications in materials science, Langmuir 10 (1994) 1498–1511, http://dx.doi.org/10.1021/la00017a030.

[27] I. Hirata, U. Zschieschang, F. Ante, T. Yokota, K. Kuribara, T. Yamamoto, K. Takimiya, M. Ikeda, H. Kuwabara, H. Klauk, T. Sekitani, T. Someya, Spatial control of the threshold voltage of low-voltage organic transistors by microcontact printing of alkyl- and fluoroalkyl-phosphonic acids, MRS Commun. 1 (2011) 33–36, http://dx.doi.org/10.1557/mrc.2011.11.

[28] L.B. Goetting, T. Deng, G.M. Whitesides, Microcontact printing of alkanephosphonic acids on aluminum: pattern transfer by wet chemical etching, Langmuir 15 (1999) 1182–1191, http://dx.doi.org/10.1021/la981094h.

[29] T. Yamamoto, K. Takimiya, Facile synthesis of highly pi-extended heteroarenes, dinaphtho[2,3-b:2′,3′-f]chalcogenopheno[3,2-b]chalcogenophenes, and their application to field-effect transistors, J. Am. Chem. Soc. 129 (2007) 2224–2225, http://dx.doi.org/10.1021/ja068429z.

[30] U. Zschieschang, F. Ante, D. Kälblein, T. Yamamoto, K. Takimiya, H. Kuwabara, M. Ikeda, T. Sekitani, T. Someya, J. Blochwitz-Nimoth, H. Klauk, Dinaphtho[2,3-b:2′,3′-f]thieno[3,2-b]thiophene (DNTT) thin-film transistors with improved performance and stability, Org. Electron. 12 (2011) 1370–1375, http://dx.doi.org/10.1016/j.orgel.2011.04.018.

[31] K. Fukuda, T. Hamamoto, T. Yokota, T. Sekitani, U. Zschieschang, H. Klauk, T. Someya, Effects of the alkyl chain length in phosphonic acid self-assembled monolayer gate dielectrics on the performance and stability of low-voltage organic thin-film transistors, Appl. Phys. Lett. 95 (2009) 203301/1–203301/3, http://dx.doi.org/10.1063/1.3259816.

[32] K. Fukuda, T. Sekitani, U. Zschieschang, H. Klauk, K. Kuribara, T. Yokota, T. Sugino, K. Asaka, M. Ikeda, H. Kuwabara, T. Yamamoto, K. Takimiya, T. Fukushima, T. Aida, M. Takamiya, T. Sakurai, T. Someya, A 4 V operation, flexible Braille display using organic transistors, carbon nanotube actuators, and organic static random-access memory, Adv. Funct. Mater. 21 (2011) 4019, http://dx.doi.org/10.1002/adfm.201101050.

[33] A. Mityashin, O.M. Roscioni, L. Muccioli, C. Zannoni, V. Geskin, J. Cornil, D. Janssen, S. Steudel, J. Genoe, P. Heremans, Multiscale modeling of the electrostatic impact of self-assembled monolayers used as gate dielectric treatment in organic thin-film transistors, ACS Appl. Mater. Interfaces 6 (2014) 15372–15378, http://dx.doi.org/10.1021/am503873f.

[34] N.G. Martinelli, M. Savini, L. Muccioli, Y. Olivier, F. Castet, C. Zannoni, D. Beljonne, J. Cornil, Modeling polymer dielectric/pentacene interfaces: on the role of electrostatic energy disorder on charge carrier mobility, Adv. Funct. Mater. 19 (2009) 3254–3261, http://dx.doi.org/10.1002/adfm.200901077.

[35] E. Delamarche, H. Schmid, A. Bietsch, N.B. Larsen, H. Rothuizen, B. Michel, H. Biebuyck, Transport mechanisms of alkanethiols during microcontact printing on gold, J. Phys. Chem. B 102 (1998) 3324–3334, http://dx.doi.org/10.1021/jp980556x.